Applied Surface Science 324 (2015) 293–299

Contents lists available at ScienceDirect

Applied Surface Science

journal homepage: www.elsevier.com/locate/apsusc

Ultralow field emission from thinned, open-ended, and defected carbon nanotubes by using microwave hydrogen plasma processing

Jian-Hua Deng[a,*], Lin Cheng[a], Fan-Jie Wang[a], Bin Yu[a], Guo-Zheng Li[a], De-Jun Li[a], Guo-An Cheng[b]

[a] College of Physics and Materials Science, Tianjin Normal University, Tianjin 300387, People's Republic of China
[b] Key Laboratory of Beam Technology and Material Modification of Ministry of Education, Beijing Normal University, Beijing 100875, People's Republic of China

ARTICLE INFO

Article history:
Received 8 September 2014
Accepted 24 October 2014
Available online 1 November 2014

Keywords:
Carbon nanotube
Microwave
Plasma
Field emission
Defect

ABSTRACT

Ultralow field emission is achieved from carbon nanotubes (CNTs) by using microwave hydrogen plasma processing. After the processing, typical capped CNT tips are removed, with thinned, open-ended, and defected CNTs left. Structural analyses indicate that the processed CNTs have more SP^3-hybridized defects as compared to the pristine ones. The morphology of CNTs can be readily controlled by adjusting microwave powers, which change the shape of CNTs by means of hydrogen plasma etching. Processed CNTs with optimal morphology are found to have an ultralow turn-on field of 0.566 V/μm and threshold field of 0.896 V/μm, much better than 0.948 and 1.559 V/μm of the as-grown CNTs, respectively. This improved FE performance is ascribed to the structural changes of CNTs after the processing. The thinned and open-ended shape of CNTs can facilitate electron tunneling through barriers and additionally, the increased defects at tube walls can serve as new active emission sites. Furthermore, our plasma processed CNTs exhibit excellent field emission stability at a large emission current density of 10.36 mA/cm^2 after being perfectly aged, showing promising prospects in applications as high-performance vacuum electron sources.

1. Introduction

High-performance field emission (FE) is of great importance in potential applications for vacuum electron emitting sources. It is often associated with low turn-on field (E_{on}, applied field at 10 μA/cm^2) and threshold field (E_{th}, applied field at 10 mA/cm^2), large current, and good stability, which requires emitters having large aspect ratios, dense and uniform emission sites, and good electrical and mechanical properties. Carbon nanotubes (CNTs), a quasi-one-dimensional material having excellent conductivity, can perfectly meet these requirements. CNTs have been intensively studied as cold field emitters since their first FE demonstration in 1995 [1–4], and have shed light on a wide range of applications such as flat panel displays [5], X-ray tubes [6], lamps [7], and field-effect transistors [8]. In comparison with other good field emitters such as nanotips [9], single-layer graphenes [10], and nanofibers [11], CNTs have lower E_{on} and E_{th} due to their incomparable large aspect ratios. However, the E_{on} of CNTs, especially for densely arrayed CNTs prepared by using chemical vapor deposition (CVD), is often larger than 1.0 V/μm [12,13], which is detrimental in practical applications. The arrayed CNTs already have advantages in large area homogeneous FE due to their uniform distribution of emission sites, it is thus essential to further lower their E_{on} and E_{th} to make them widely applicable. Great efforts have been paid on lowering the operation field of CNTs in recent years. Typical approaches are decreasing the work function of emitters by element doping [14], introducing new active emission sites by ion irradiation and composition [4,12,13], chemical processing [15], and so on. Plasma treatment is another widely employed strategy. For example, Chen at al reported the FE properties of NH_3 plasma processed CNTs, and they found that the treated CNTs have a much lower E_{on} than that of the untreated ones [16]. Similar strategies have also been used to improve the FE properties of CNTs, such as oxygen [17,18] and nitrogen processing [19,20]. However, there are still great efforts need to be made to further lower the E_{on} and E_{th}, ameliorate the FE stability, and deeply understand the FE enhancement mechanism.

In the present study, we prepared CVD CNTs and processed them by using microwave hydrogen plasma. Thinned, open-ended, and defected CNTs were obtained after the processing. We studied their FE properties and found that the processed CNTs have far better FE

* Corresponding author. Tel.: +86 22 23766519; fax: +86 22 23766519.
E-mail address: jhdeng1983@163.com (J.-H. Deng).

http://dx.doi.org/10.1016/j.apsusc.2014.10.137
0169-4332/

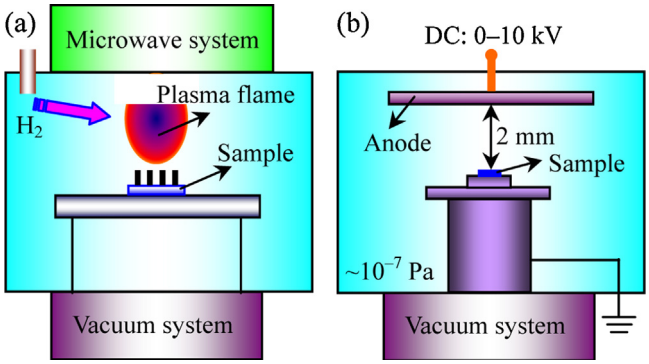

Fig. 1. (a) Schematic of the microwave system used for the hydrogen plasma processing on CNTs. (b) Schematic of the diode-type setup used for the FE tests.

performance than that of the as-grown ones, and we also proposed a mechanism to illustrate this FE improvement.

2. Experimental details

2.1. Sample preparation

CNTs are prepared in a tubular furnace with C_2H_2 as the carbon feedback by using a classical thermal CVD approach. This has been described in detail in our previous studies [4,12] and can also be found in 'Methods' of the Supplementary information (including Figs. S1 and S2). The hydrogen plasma processing on CNTs was performed in a vacuum chamber at room temperature by using a microwave (2.45 GHz) plasma system, as schematically shown in Fig. 1(a). The CNTs were placed on a graphite specimen holder. The hydrogen plasma processing was taken under 10 sccm H_2 at 1 kPa. The distance between the plasma flame and our samples was ~1 cm. The morphology of the processed CNTs was mainly controlled by adjusting the processing time and microwave powers. After then, samples were cooled to room temperature in H_2 ambient.

2.2. Structural characterization

Morphological changes to CNTs due to the hydrogen plasma processing were studied by using scanning electron microscopy (SEM, S-4800, Hitachi, Japan) imaging with an accelerating voltage of 10 kV. Transmission electron microscope (TEM, JEM-2010, JEOL, Japan, 200 kV) was used to observe the fine structure of our samples. The defect analysis was performed by using Raman spectroscopy (LabRAM Aramis, Horiba Jobin Yivon, France) with a He–Ne laser (wavelength: 633 nm) in atmosphere and X-ray photoelectron spectroscopy (XPS, PHI Quantera SXM) using Al Kα irradiation (~1486.6 eV). The work function of our samples was measured by using a photoelectron spectrometer (AC-2, Riken Keiki, Japan, spot area: 4 mm × 4 mm) at ambient pressure.

2.3. FE tests

The FE tests of CNTs were performed by using a conventional diode-type setup in a vacuum chamber (~1×10^{-7} Pa), as schematically shown in Fig. 1(b). The prepared samples were used as the cathode against a stainless steel plate as the anode, and the cathode–anode gap was 2 mm. During the FE tests, a DC voltage ranging from 0 to 10 kV was applied on the anode with a constant increasing rate of 500 V/min while grounding the cathode. The FE results were automatically recorded by a computer in terms of emission current *versus* applied voltage.

3. Results and discussion

3.1. CNTs in different processing stages

The morphology of CNTs in different processing stages was observed by using SEM, as shown in Fig. 2. In this research, the microwave power is 400 W. The tips of as-grown CNTs are 40–60 nm in diameter, ~22 μm in length, densely arrayed, and have curved tips and smooth surfaces (Fig. 2(a) and (b)). While that for the 30-min processed CNTs are 20–40 nm in diameter, ~18 μm in

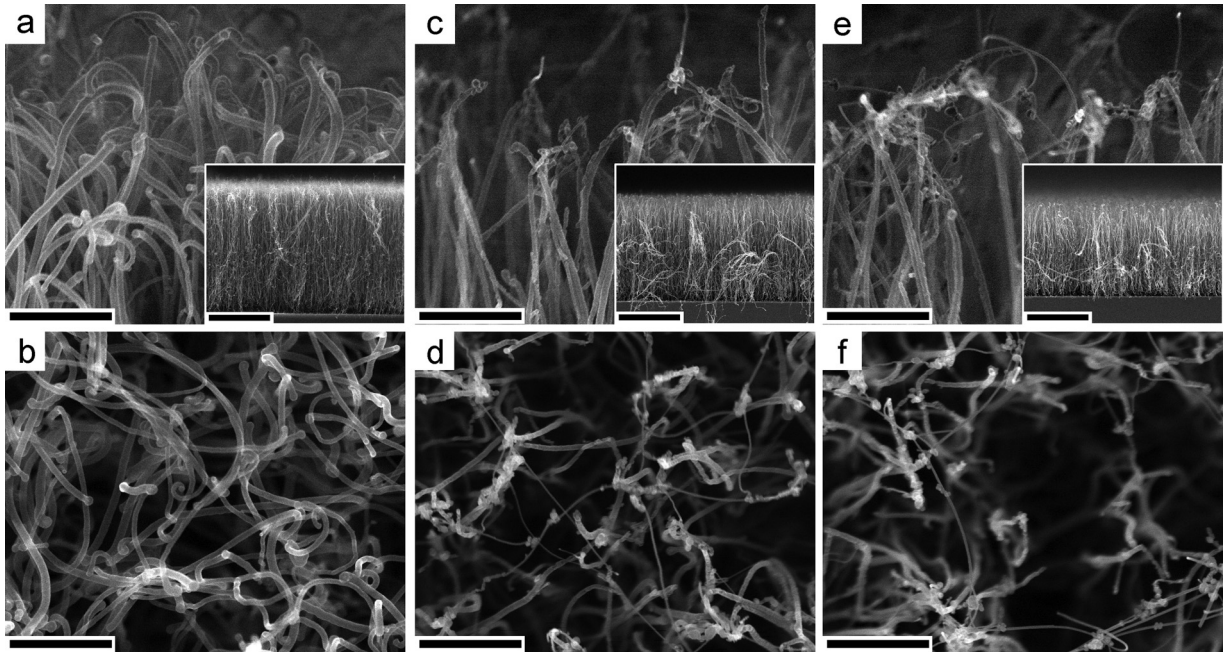

Fig. 2. Side-view SEM images of hydrogen plasma processed CNTs for (a) 0 min, (c) 30 min, and (e) 60 min. The insets are the corresponding low-resolution side-view SEM images showing the length of CNTs. Top-view SEM images of the processed CNTs for (b) 0 min, (d) 30 min, and (f) 60 min. Scale bars in (a–f) are 500 nm, in the insets of (a, c, e) are 10 μm.

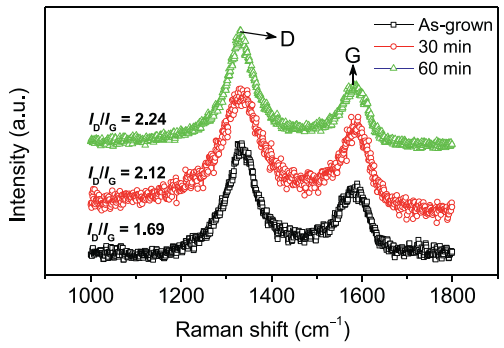

Fig. 3. Raman spectra of the as-grown CNTs and CNTs processed in 30 and 60 min. The I_D/I_G is the intensity ratio of the D peak (centered at ~1334 cm^{-1}) and the G peak (centered at ~1585 cm^{-1}).

length, relatively sparsely distributed, and severely defected, as shown in Fig. 2(c) and (d). In addition, the pristine curved CNT tips are removed by the plasma (Fig. 2(b)), with a few ultrathin CNTs lying on the surface of the array (Fig. 2(d)). The morphology change of CNTs with further increasing the processing time to 60 min is not obvious except that the length of CNTs decreases to ~16 μm (Fig. 2(e) and (f)). We attribute this length change to the hydrogen plasma etching on our carbon materials, which has been well-reported in previous studies [21,22]. The above results indicate that the hydrogen plasma processing can bring defects to CNTs, thin CNT tips, and shorten CNTs.

The defects of CNTs are characterized by using Raman spectroscopy (laser wavelength: 633 nm) and XPS. Fig. 3 shows Raman spectra of the as-grown CNTs and CNTs processed in 30 and 60 min. For all types of CNTs, they have two typical Raman peaks: a D-peak centered at ~1334 cm^{-1} and a G-peak centered at ~1585 cm^{-1}. The D-peak corresponds with the defected graphite in CNTs while the G-peak arises from the ordered one [23–25]. The intensity ratio of the D peak and G peak (I_D/I_G) is often used to qualitatively evaluate the defect of CNTs [23]. The I_D/I_G ratios for the as-grown CNTs, and CNTs processed in 30 and 60 min are 1.69, 2.12, and 2.24, respectively. In comparison with the as-grown CNTs, this slight increase of I_D/I_G ratio indicates that a small amount of defects are introduced to CNTs after the plasma processing, which is quite different from the ion irradiation on CNTs reported previously that brings plenty of defects to CNTs [4,26]. It is interesting that the increase of I_D/I_G ratio is negligible when the processing time is prolonged from 30 min to 60 min. We attribute this to the high etching rate of hydrogen plasma on CNTs in our processing conditions that makes the residual CNTs have similar defect levels before being removed.

XPS spectra can provide the chemical bonding information of CNTs and thus can help us deeply understand their microstructure. Fig. 4(a) shows the XPS spectrum of the C1s peak for the as-grown CNTs. The XPS spectra for CNTs processed in 30 and 60 min are shown in Fig. S3 of the Supplementary information. De-convolution of the C1s peaks shows three component peaks centered at 284, 285, and 288 eV, which arise from the C—C SP^2 hybridization [27], C—C SP^3 hybridization [28], and oxygen contamination [29], respectively. Since CNT is mainly a SP^2-hybridized carbon network, the fraction of SP^3-hybridized carbon (SP^3%) can thus be used to roughly characterize the amount of defects. And, in comparison with the planar SP^2-hybridized carbon, the distorted SP^3-hybridized carbon is believed to be helpful for FE [30]. However, too many defects will also deteriorate the electrical properties of CNTs. The SP^3% values of the processed CNTs are slightly larger than that of the as-grown ones, as shown in Fig. 4(b), indicating that the plasma processing introduces a small amount of defects to our CNTs. We consider that this slight increase of defects will not only facilitate the FE of CNTs but also reserve their excellent electrical properties. Furthermore, the SP^2% and SP^3% values of the 30 min sample are similar to those of the 60 min one, indicating that the processed CNTs are in similar defect levels over a certain processing time. This is in good agreement with our previous Raman analysis that the I_D/I_G ratios of these two types of samples show no much difference.

The fine structure of our samples was characterized by using a TEM. As-grown CNTs and CNTs processed in 30 min were chosen to perform the TEM observation for comparison. Fig. 5(a) shows a low-resolution TEM image of a capped as-grown CNT. This CNT has a thick tip of ~77 nm in diameter and a typical hollow core. CNTs thin greatly after the 30 min plasma processing and the capped structure is removed with open ends left, as shown in Fig. 5(b). Fig. 5(c) and (d) shows the fine structure of tube walls of an as-grown CNT and a processed one, respectively. Their layers are ~60 and ~40, respectively, further indicating the thinning of CNTs after the plasma processing. High-resolution TEM images of much thinner processed CNTs can also be found in Fig. S4 of the Supplementary information. Additionally, the surface topography of these two types of CNTs is different. The as-grown CNT has a uniform and relatively smooth surface while that for the processed one is inhomogenous and bumpy. We consider that these defects can serve as new active emission sites during FE and thus enhance the FE performance of CNTs.

3.2. The influence of microwave powers on the morphology of CNTs

Fig. 6(a) and (b) shows top-view SEM images of CNTs processed at 200 and 600 W for 60 min, respectively. In comparison with the CNTs processed at 400 W, as shown in Fig. 2(e) and (f), the 200 W sample has more ultrathin CNTs lying down on the top surface of the array. This is ascribed to the relatively weak hydrogen plasma

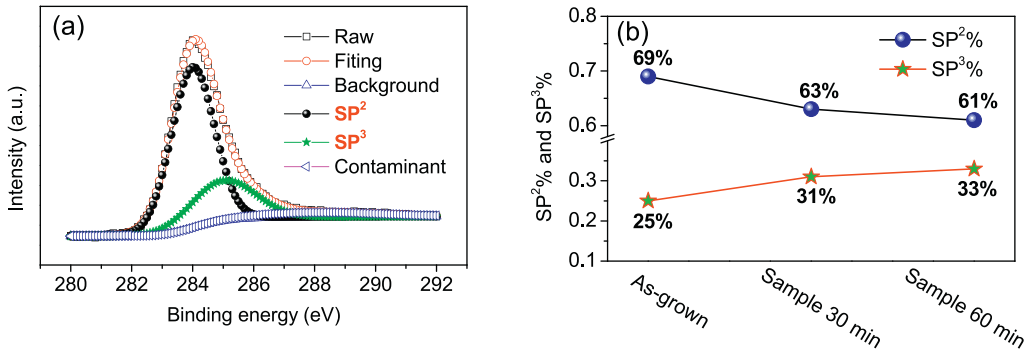

Fig. 4. XPS spectrum of the C1s peak for the as-grown CNTs, which has three component peaks centered at 284, 285, and 288 eV. (b) The intensity fractions of the SP^2- and SP^3-hybridized carbon of our samples.

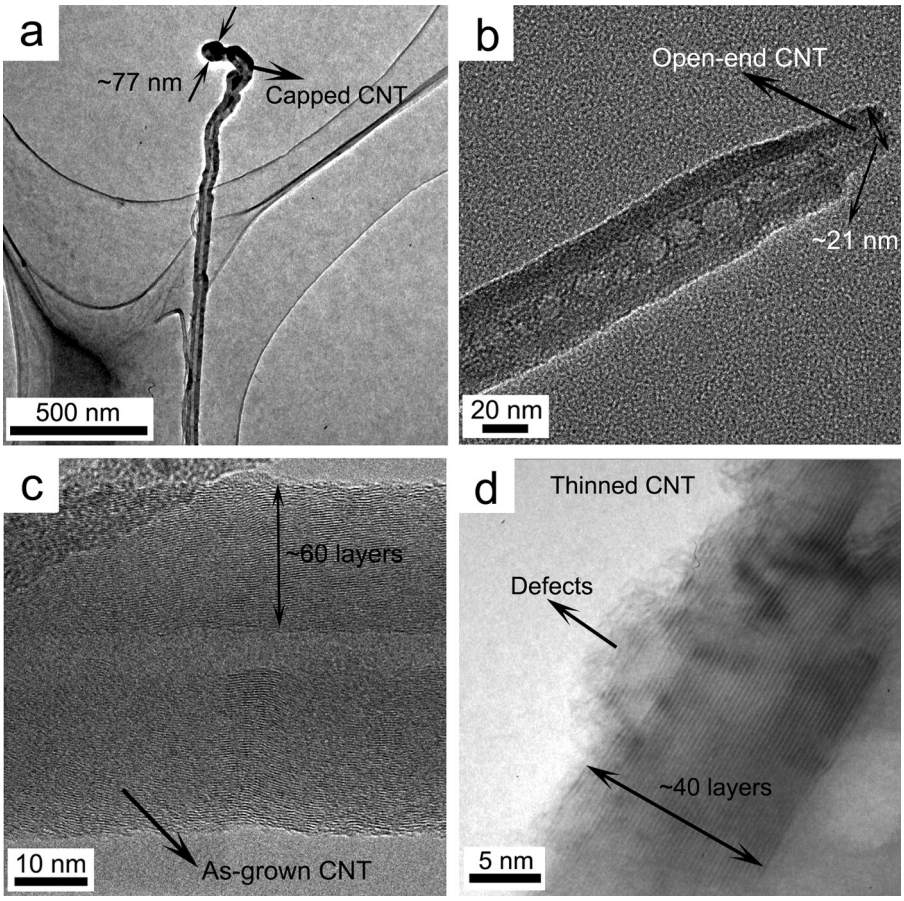

Fig. 5. Low-resolution TEM images of (a) a capped as-grown CNT and (b) a thinned and open-ended processed CNT. High-resolution TEM images of (c) an as-grown CNT with ~60 layers and (d) a processed CNT with ~40 layers and defected outer shells.

etching in the 200 W condition, resulting in that more CNTs are reserved with their outer shells being etched away. We consider that this flat-lying CNT net contributes less in improving the FE behavior of CNTs because the horizontally distributed CNTs have far smaller aspect ratios than that of the vertically aligned ones. The 600 W sample by contrast (Fig. 6(b)), has morphology similar to the 400 W sample but with relatively less ultrathin CNTs, suggesting that the etching of CNTs is more intense in this condition. We have further increased the microwave power to 1200 W and found that nearly all CNTs were removed after being processed for 60 min, as shown in Fig. S5 of the Supplementary information. In a word, the microwave power influences the morphology of CNTs by means of plasma etching, and we can readily obtain our anticipated CNT morphology by merely adjusting microwave powers.

3.3. FE performance of the processed CNTs

FE properties of as-grown CNTs and processed CNTs with typical morphology were tested for comparison. Three types of processed CNTs are chosen: (1) 400 W for 30 min; (2) 400 W for 60 min; (3) 200 W for 60 min. We name them here as sample 30 min, sample 60 min, and sample 200 W for convenience. The differences among these samples are that the sample 30 min and sample 60 min have difference in length (insets of Fig. 2(c) and (e)), and the sample 200 W has an ultrathin CNT net covered on the top surface of the array (Fig. 6(a)). Fig. 7 shows FE properties of the four types of CNTs above mentioned, presented in terms of emission current density (J) *versus* applied field (E), *i.e.*, the J–E curves. It should be emphasized that these J–E curves were obtained right after an aging process, in which continuous FE at constant applied fields was performed on CNTs for 5 h when the J is around 10 mA/cm^2. This aging process is helpful for removing any absorbates on CNTs and burning out loosely bonded CNTs [31,32]. The corresponding FE results are shown in Table 1. It can be seen that the E_{on} and E_{th} for the processed CNTs are far smaller than those for the as-grown ones, indicating that the plasma processing ameliorates the FE performance of our emitters. Sample 60 min has the optimal FE properties. It has an ultralow E_{on} of 0.566 V/μm and E_{th} of 0.896 V/μm. Considering the high density of our CNTs, this FE performance is outstanding. It is far better than a great many well reported CNT emitters such as ion irradiated CNTs [4], CNT–graphene composites [12,13], element doped CNTs [14], chemically processed CNTs [15], NH_3, oxygen, and nitrogen processed CNTs [16–20]. Replotting of the data as $\ln(J/E^2)$ *versus* $1/E$, *i.e.*, the F–N plots, as shown in the inset of Fig. 7, indicates typical F–N type FE behavior [33]. The work function (Φ) of our samples was determined by using a photoelectron spectrometer. The Φ values of the processed CNTs (4.75–4.79 eV) are slightly smaller than that of the as-grown ones (4.89 eV), which is attributed to the fact that the Fermi level is promoted by the increased state density of defects after the plasma processing [34].

Table 1
FE testing results of our samples. Φ is the work function and β is the field enhancement factor. The 60 min sample (bolded) has the best FE performance.

Samples	E_{on} (V/μm)	E_{th} (V/μm)	Φ (eV)	β
As-grown	0.948	1.559	4.89	3414
30 min	0.617	0.948	4.77	6495
60 min	**0.566**	**0.896**	**4.75**	**7504**
200 W	0.804	1.124	4.79	4041

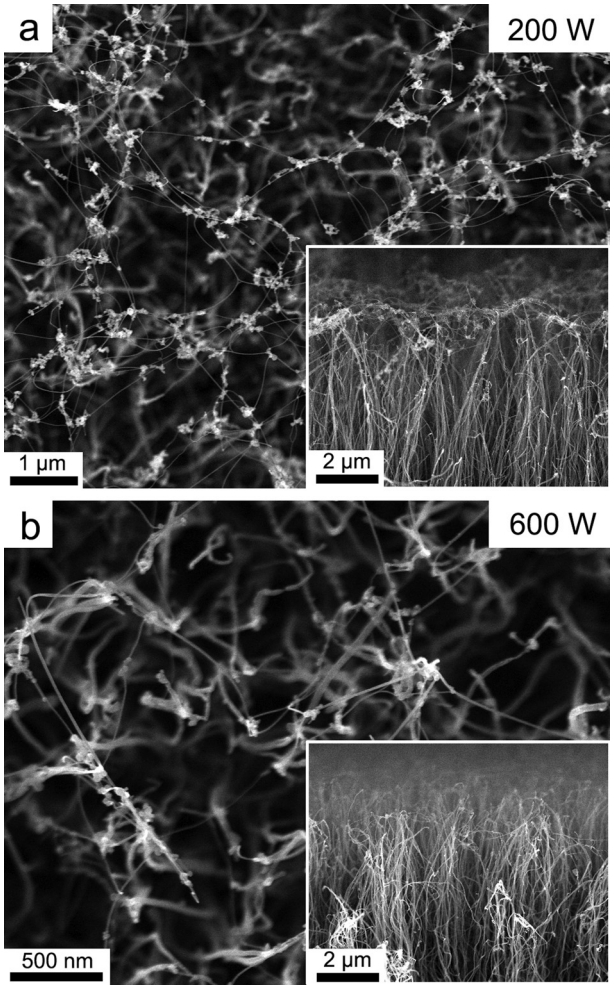

Fig. 6. Top-view SEM images of CNTs processed at (a) 200 W and (b) 600 W. The insets are the corresponding side-view SEM images. The processing time is 60 min.

With Φ and the constant slopes of the *F–N* plots in the low-*E* regions, the field enhancement factor (β) for our samples can be determined by following the *F–N* theory [33]. The sample 60 min has the largest β (~7504), far larger than that of the as-grown CNTs (~3414). Together with the FE *J–E* curves above presented, it can be found that the FE performance of CNTs is mainly determined by the β factors. Additionally, the sample 30 min, ~18 μm in length, has a smaller β (~6495) than that of the sample 60 min (~7504), which is ~16 μm in length, suggesting that the β factor is not merely

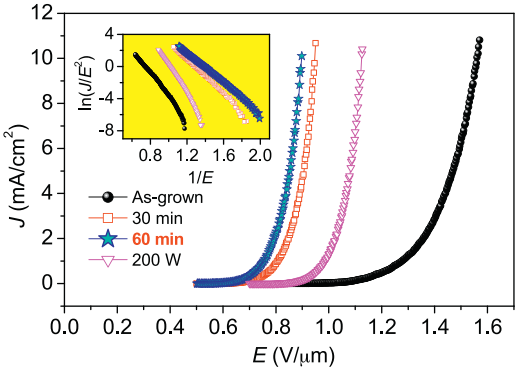

Fig. 7. FE *J–E* curves of the as-grown CNTs, and CNTs processed in 30 and 60 min, and at 200 W. The inset is the corresponding *F–N* plots given in terms of $\ln(J/E^2)$ *versus* $1/E$.

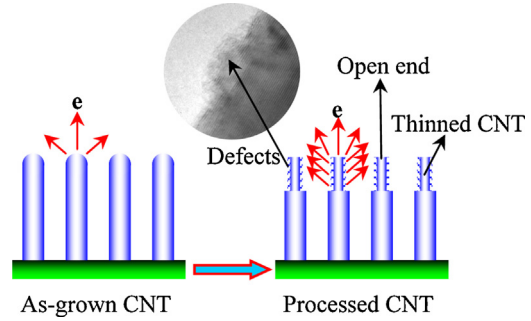

Fig. 8. Schematic illustration for the FE improvement of CNTs after the hydrogen plasma processing. The "e" represents emitted electrons.

dependent on the aspect ratios of emitters. We consider that the β is a composite factor related to both the aspect ratio and the number of active emission sites of emitters. Furthermore, we should also take the field screening effect into consideration due to the high density of our emitters [35], which means that the β is not directly determined by the actual ratio of length to diameter. In comparison with the sample 30 min and sample 60 min, the deteriorated FE performance from the sample 200 W is ascribed to the screening of the horizontally distributed ultrathin CNT net that hinders the electron emitting from the underneath CNT arrays.

Fig. 8 schematically illustrates the FE improvement of CNTs after the hydrogen plasma processing. As discussed above, the enhanced FE performance is mainly due to the structural change of CNTs rather than the decrease of work function. We consider that there are two major structural changes. First, in comparison with the smooth spherical surface of the as-grown CNTs, the thinned and open-ended shape of the processed CNTs can yield far larger local applied fields at emission sites and thus facilitate the electron tunneling through barriers [3]. Second, the defects at the tube walls of processed CNTs can also serve as new active emission sites, which will greatly increase electron transferring traces [30]. For example, electron transferring mainly occurs at the tip of a defect-free CNT, as shown in Fig. 8, but for a defected one, the distorted SP^3-hybridized defects at tube walls can also emit electrons. This increase of electron transferring traces will greatly improve the FE properties of emitters. In a word, both the shape change and the microstructure change of CNTs will enhance their FE performance.

Longtime stable FE at J_{th} (threshold emission current density, 10 mA/cm^2) is of great importance in practical applications. In this research, FE stability of the as-grown CNTs and the sample 60 min, which has the best FE *J–E* performance, was measured for comparison. Fig. 9 shows the 20-h FE stability of these two types of samples at ~J_{th}. The experimental data is plotted in terms of *J versus* time. The current density degradation is characterized by using a

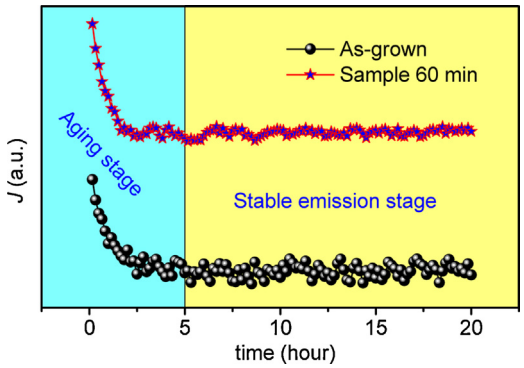

Fig. 9. 20-h FE stability of the as-grown CNTs and the CNTs processed at 400 W for 60 min (sample 60 min), presented in terms of *J versus* time.

Table 2
FE stability testing results of the as-grown CNTs and the CNTs processed at 400 W for 60 min (sample 60 min). J_{mean} is the mean emission current density, E is the constant fields applied on samples during the stability tests, $J_{drop,1}$ and $J_{drop,2}$ are the current density degradation in the first 5 h (aging stage) and the last 15 h (stable emission stage), respectively. The "+" and "−" represent the current decrease and increase during stability tests, respectively.

Samples	J_{mean} (mA/cm^2)	E (V/μm)	$J_{drop,1}$ (%)	$J_{drop,2}$ (%)
As-grown	10.39	1.60	+19.4	+0.4
60 min	10.36	0.95	+24.0	−1.6

parameter: J_{drop}, which is calculated by $(J_{first} - J_{last})/J_{mean}$, where the J_{first}, J_{last}, and J_{mean} are the first, the last, and the mean emission current density in a certain testing duration. The corresponding FE stability testing results are shown in Table 2. It can be seen that the current degradation in the first 5 h is dramatic while it is negligible in the last 15 h, and we name the J_{drop} in these two durations as $J_{drop,1}$ and $J_{drop,2}$. The $J_{drop,1}$ values of the as-grown CNTs and the sample 60 min are 19.4% and 24.0%, respectively. This great current degradation is attributed to the Joule heating induced burning out of active emission sites [32], which is helpful for the aging of our samples, thus the first 5 h is actually the aging stage. Furthermore, the $J_{drop,1}$ of the sample 60 min is larger than that of the as-grown CNTs. We attribute this to that the processed CNTs have a great many defected and thinned CNTs, and these CNTs are more likely to be burned out during the longtime large current FE. After being perfectly aged, the electron emission is nearly stable, as seen from the J–time curves of the last 15 h shown in Fig. 9 (stable emission stage) and the small $J_{drop,2}$ (<1.6%) shown in Table 2. It should be emphasized that the operation E of the sample 60 min is only 0.95 V/μm, far smaller than 1.60 V/μm of the as-grown CNTs, which is quite essential in practical applications. Furthermore, in comparison with the as-grown CNTs, the current fluctuation of the processed CNTs is smaller. We attribute this to the uniform tip morphology of the processed CNTs that provide a homogeneous array of active emission sites, which is quite different from the curved and sparely distributed tips of the as-grown CNTs (Fig. 2(b)).

4. Conclusions

Thinned, open-ended, and defected CNTs were obtained by using microwave hydrogen plasma processing on CVD prepared CNT arrays. Based on Raman, XPS, and TEM analyses, we find that the processed CNTs have more SP^3-hybridized defects as compared to as-grown ones, and these defects are widely distributed on the tube walls. The shape of CNTs can be adjusted by changing microwave powers, mainly due to that the hydrogen plasma etching rate on CNTs is microwave power dependent. The FE study indicates that the processed CNTs have superior FE performance to that of the as-grown ones. This improved FE is ascribed to, first, the open-ended and thinned shape of CNTs that promotes the local applied fields at emission sites and second, the increased SP^3-hybridized defects that introduces new active emission sites to our emitters. Optimal FE properties are obtained from a processed CNT array. It has an ultralow E_{on} of 0.566 V/μm and E_{th} of 0.896 V/μm, much better than those of the as-grown CNTs. The FE stability study shows that stable FE can be achieved by perfectly pre-aging our samples. The ultralow E_{on} and E_{th}, and the excellent FE stability at $\sim J_{th}$ have made our hydrogen plasma processed CNTs an excellent FE material in potential applications for vacuum electron sources.

Acknowledgments

This work was supported by the National Natural Science Foundation of China for Youth Science Funds (51302187) and the Key Project of Tianjin Natural Science Foundation (14JCZDJC32100). JHD also thanks the financial support from the Tianjin Key Laboratory of Structure and Performance for Functional Molecule and the "131" Innovative Talents cultivation of Tianjin.

Appendix A. Supplementary data

Supplementary data associated with this article can be found, in the online version, at http://dx.doi.org/10.1016/j.apsusc.2014.10.137.

References

[1] W.A. de Heer, A. Châtelain, D. Ugarte, A carbon nanotube field-emission electron source, Science 270 (1995) 1179–1180.
[2] S.S. Fan, M.G. Chapline, N.R. Franklin, T.W. Tombler, A.M. Cassell, H.J. Dai, Self-oriented regular arrays of carbon nanotubes and their field emission properties, Science 283 (1999) 512–514.
[3] L.B. Zhu, Y.Y. Sun, D.W. Hess, C.P. Wong, Well-aligned open-ended carbon nanotube architectures: an approach for device assembly, Nano Lett. 6 (2006) 243–247.
[4] J.H. Deng, X.G. Hou, L. Cheng, F.J. Wang, B. Yu, G.Z. Li, D.J. Li, G.A. Cheng, S.L. Wu, Irradiation damage determined field emission of ion irradiated carbon nanotubes, ACS Appl. Mater. Interfaces 6 (2014) 5137–5143.
[5] Q.H. Wang, M. Yan, R.P.H. Chang, Flat panel display prototype using gated carbon nanotube field emitters, Appl. Phys. Lett. 78 (2001) 1294–1296.
[6] A. Haga, S. Senda, Y. Sakai, Y. Mizuta, S. Kita, F. Okuyama, A miniature X-ray tube, Appl. Phys. Lett. 84 (2004) 2208–2210.
[7] Y. Saito, S. Uemura, Field emission from carbon nanotubes and its application to electron sources, Carbon 38 (2000) 169–182.
[8] L. Ding, Z.X. Wang, T. Pei, Z.Y. Zhang, S. Wang, H.L. Xu, F. Peng, Y. Li, L.M. Peng, Self-aligned U-gate carbon nanotube field-effect transistor with extremely small parasitic capacitance and drain-induced barrier lowering, ACS Nano 5 (2011) 2512–2519.
[9] C.L. Tsai, C.F. Chen, L.K. Wu, Bias effect on the growth of carbon nanotips using microwave plasma chemical vapor deposition, Appl. Phys. Lett. 81 (2002) 721–723.
[10] Z.S. Wu, S.F. Pei, W.C. Ren, D.M. Tang, L.B. Gao, B.L. Liu, F. Li, C. Liu, H.M. Cheng, Field emission of single-layer graphene films prepared by electrophoretic deposition, Adv. Mater. 21 (2009) 1756–1760.
[11] C.H. Weng, K.C. Leou, H.W. Wei, Z.Y. Juang, M.T. Wei, C.H. Tung, C.H. Tsai, Structural transformation and field emission enhancement of carbon nanofibers by energetic argon plasma post-treatment, Appl. Phys. Lett. 85 (2004) 4732–4734.
[12] J.H. Deng, R.T. Zheng, Y. Zhao, G.A. Cheng, Vapor-solid growth of few-layer graphene using radio frequency sputtering deposition and its application on field emission, ACS Nano 6 (2012) 3727–3733.
[13] J.H. Deng, G.A. Cheng, R.T. Cheng, B. Yu, G.Z. Li, X.G. Hou, M.L. Zhao, D.J. Li, Catalyst-free, self-assembly, and controllable synthesis of graphene flake–carbon nanotube composites for high-performance field emission, Carbon 67 (2014) 525–533.
[14] G. Zhang, W.H. Duan, B.L. Gu, Effect of substitutional atoms in the tip on field-emission properties of capped carbon nanotubes, Appl. Phys. Lett. 80 (2002) 2589–2591.
[15] S.C. Kung, K.C. Hwang, I.N. Lin, Oxygen and ozone oxidation-enhanced field emission of carbon nanotubes, Appl. Phys. Lett. 80 (2002) 4819–4821.
[16] G.H. Chen, S. Neupane, W.Z. Li, L.N. Chen, J.D. Zhang, An increase in the field emission from vertically aligned multiwalled carbon nanotubes caused by NH_3 plasma treatment, Carbon 52 (2013) 468–475.
[17] A. Mathur, S.S. Roy, K.S. Hazra, S. Wadhwa, S.C. Ray, S.K. Mitra, D.S. Misra, J.A. McLaughlin, Oxygen plasma assisted end-opening and field emission enhancement in vertically aligned multiwall carbon nanotubes, Mater. Chem. Phys. 134 (2012) 425–429.
[18] G. Sanborn, S. Turano, W.J. Ready, Oxygen plasma resurrection of triode type carbon nanotube field emission cathode, Diamond Relat. Mater. 43 (2014) 1–4.
[19] D.H. Lee, J.A. Lee, W.J. Lee, S.O. Kim, Flexible field emission of nitrogen-doped carbon nanotubes/reduced graphene hybrid films, Small 7 (2011) 95–100.
[20] B.B. Wang, Q.J. Cheng, X. Chen, K. Ostrikov, Enhancement of electron field emission of vertically aligned carbon nanotubes by nitrogen plasma treatment, J. Alloys Compd. 509 (2011) 9329–9334.
[21] A. Hassanien, M. Tokumoto, P. Umek, D. Vrbanič, D. Mihailović, P. Venturini, S. Pejovnik, Selective etching of metallic single-wall carbon nanotubes with hydrogen plasma, Nanotechnology 16 (2005) 278–281.
[22] A. Okita, Y. Suda, A. Oda, J. Nakamura, A. Ozeki, K. Bhattacharyya, H. Sugawara, Y. Sakai, Effects of hydrogen on carbon nanotube formation in CH_4/H_2 plasmas, Carbon 45 (2007) 1518–1526.
[23] F. Tuinstra, J.L. Koenig, Raman spectrum of graphite, J. Chem. Phys. 53 (1970) 1126–1130.
[24] A.C. Ferrari, J.C. Meyer, V. Scardaci, C. Casiraghi, M. Lazzeri, F. Mauri, S. Piscanec, D. Jiang, K.S. Novoselov, S. Roth, A.K. Geim, Raman spectrum of graphene and graphene layers, Phys. Rev. Lett. 97 (2006) 187401.
[25] R.J. Nemanich, S.A. Solin, First- and second-order Raman scattering from finite-size crystals of graphite, Phys. Rev. B 20 (1979) 392–401.

[26] J.H. Deng, Z.X. Ping, R.T. Zheng, G.A. Cheng, Electron transferring from titanium ion irradiated carbon nanotube arrays into vacuum under low applied fields, Nucl. Instrum. Methods Phys. Res. B 269 (2011) 1082–1087.
[27] R. Bertoncello, A. Casagrande, M. Casarin, A. Glisenti, E. Lanzoni, L. Mirenghi, E. Tondello, Tin, Tic and Ti (C, N) film characterization and its relationship to tribological behaviour, Surf. Interface Anal. 18 (1992) 525–531.
[28] P. Sundberg, R. Larsson, B. Folkesson, On the core electron binding energy of carbon and the effective charge of the carbon atom, J. Electron Spectrosc. Relat. Phenom. 46 (1988) 19–29.
[29] D. Rats, L. Vandenbulcke, R. Herbin, R. Benoit, R. Erre, V. Serin, J. Sevely, Characterization of diamond films deposited on titanium and its alloys, Thin Solid Films 270 (1995) 177–183.
[30] G. Wei, Emission property of carbon nanotube with defects, Appl. Phys. Lett. 89 (2006) 143111.
[31] A. Maiti, J. Andzelm, N. Tanpipat, P. von Allmen, Effect of adsorbates on field emission from carbon nanotubes, Phys. Rev. Lett. 87 (2001) 155502.
[32] K.A. Dean, T.P. Burgin, B.R. Chalamala, Evaporation of carbon nanotubes during electron field emission, Appl. Phys. Lett. 79 (2001) 1873–1875.
[33] R.H. Fowler, L. Nordheim, Electron emission in intense electric fields, Proc. R. Soc. Lond. Ser. A 119 (1928) 173–181.
[34] G. Kim, B.W. Jeong, J. Ihm, Deep levels in the band gap of the carbon nanotube with vacancy-related defects, Appl. Phys. Lett. 88 (2006) 193107.
[35] J.S. Suh, K.S. Jeong, J.S. Lee, I. Han, Study of the field-screening effect of highly ordered carbon nanotube arrays, Appl. Phys. Lett. 80 (2002) 2392–2394.